Controlling the Supramolecular Polymerization of Squaraine Dyes by a Molecular Chaperone Analogue

Lara Kleine-Kleffmann,[†] Vladimir Stepanenko,[†,‡] Kazutaka Shoyama,[‡] Marius Wehner,[†] Frank Würthner[†,‡,*]

† Institut für Organische Chemie, Universität Würzburg, Am Hubland, 97074 Würzburg, Germany

‡ Center for Nanosystems Chemistry & Bavarian Polymer Institute, Universität Würzburg, Theodor-Boveri-Weg, 97074 Würzburg, Germany

KEYWORDS. dye aggregates, molecular chaperone, self-assembly, supramolecular polymerization, squaraines.

ABSTRACT: Molecular chaperones are proteins that assist the (un)folding and (dis)assembly of other macromolecular structures towards their biologically functional state in a non-covalent manner. Transferring this concept from nature to artificial self-assembly processes, here we show a new strategy to control supramolecular polymerization via a chaperone-like two-component system. A new kinetic trapping method was developed which enables efficient retardation of the spontaneous self-assembly of a squaraine dye monomer. The suppression of supramolecular polymerization could be regulated with a cofactor which precisely initiates self-assembly. The presented system was investigated and characterized by UV/vis, FTIR and NMR spectroscopy, atomic force microscopy (AFM), isothermal titration calorimetry (ITC) and single crystal X-ray diffraction. With these results living supramolecular polymerization and block copolymer fabrication could be realized, demonstrating a new possibility for effective control over supramolecular polymerization processes.

Introduction

Taking inspiration from nature's sophisticated macromolecular entities, many supramolecular materials[1] ranging from artificial molecular machines[2] to supramolecular polymers[3-5] have been synthesized in the last years. In this regard, supramolecular polymers have emerged as promising new materials with interesting mechanical or functional properties[6,7] since the first introduction of the term by Lehn and co-workers in 1990.[8] Remarkable control over supramolecular polymerization was achieved by gaining deep insights into the thermodynamics and kinetics of such processes.[9-12] By understanding the pathway complexity of supramolecular architectures,[13] (seeded) living supramolecular polymerization could be achieved.[14-16] Here, an essential milestone was the generation of kinetically trapped species e.q. through intramolecular hydrogen bonding,[14-16] photoisomerization,[17] solvent processing,[18,19] or a combination of several techniques.[20,21] In order to initiate supramolecular polymerization in such kinetically trapped systems, aggregate seeds,[22-24] molecular initiators[14] or external stimuli have been used. With this groundwork, the synthesis of supramolecular block copolymers could also be achieved most recently.[25-28]

Herein, we introduce a new kinetic trapping strategy, i.e. a new method to suppress spontaneous nucleation of monomers inspired by the sophisticated supramolecular systems found in nature where complex self-assembly processes are assisted by molecular chaperones. Molecular chaperones non-covalently support the folding and assembly processes of other macromolecular systems to reach their functionally active conformation, the so-called native state.[29] They are not present in the final structure and don't provide the sterical information for correct folding or assembly of the proteins. In general, their modus operandi is based on the inhibition of unproductive protein interactions, in doing so they facilitate the formation of functional assemblies.[30] Properties of that kind are not only restricted to proteins,[31] chaperone-like activity was also discovered in small organic molecules, so called pharmacological[32] and chemical chaperones.[33]

In this article, the idea of an artificial chaperone was transferred from protein assembly to the self-assembly of synthetic supramolecular polymers. The idea to control supramolecular self-assembly processes by chaperone-like molecules has been discussed in literature for several years.[10,11] A few examples where supramolecular polymerization is mediated by additives are known,[34] but often the resulting supramolecular assemblies are co-aggregates,[35,36] whereas molecular chaperones are neither part of nor dictate the final supramolecular structure. Chiral organic cages have shown promise as chirality inducing catalysts for supramolecular polymerization.[37]

Here, the goal was to develop an artificial two-component chaperone system to control the supramolecular polymerization process of a synthetic squaraine dye building block. Following this idea, the squaraine dye monomers are kinetically trapped through complexation with an artificial molecular chaperone (Figure 1, red arrow) and thereby disabled from spontaneous polymerization. For this purpose a tetralactam macrocycle was employed, a compound class which is known in literature for its

use as rotaxane-wheel for many squaraine dyes.[38] Control over supramolecular polymerization can now be achieved by the removal of the macrocycle by addition of an initiator (decomplexation, orange arrow). In this regard, suitable cofactors with a high binding affinity to tetralactam macrocycles are diketopiperazines.[39] The squaraine dye monomers are set free again and able to form supramolecular polymers via π–π-stacking (light blue) and hydrogen bonding (dark blue) interactions.

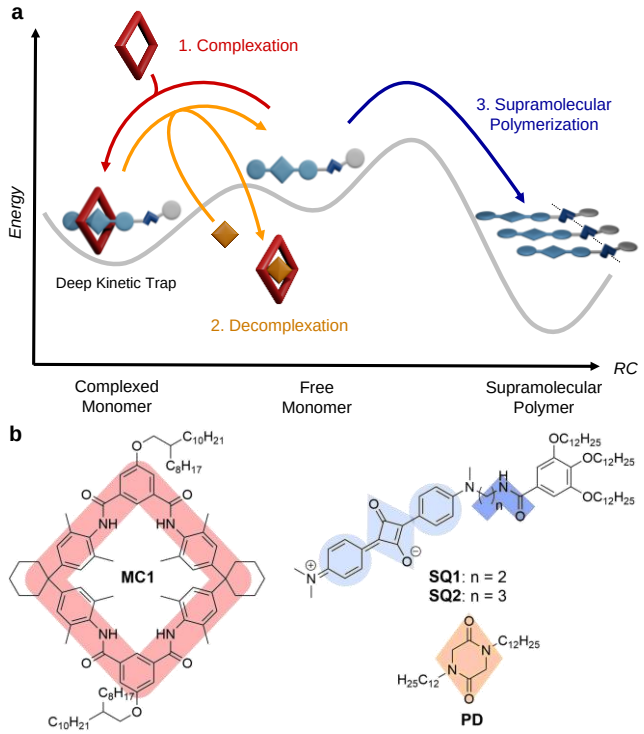

Figure 1. a) Schematic energy landscape of a supramolecular polymerization. 1.) Through complexation with a molecular chaperone analogue (red) the dye monomers are kinetically trapped and spontaneous supramolecular polymerization is inhibited. 2.) Removal of the molecular chaperone analogue through addition of a better binding guest molecule (orange). 3.) The free monomers self-assemble via π–π-interactions (light blue) and hydrogen bonding (dark blue) into supramolecular polymers. b) Chemical structures of squaraines **SQ1** and **SQ2**, tetralactam macrocycle **MC1** and 1,4-dodecyl-2,5-piperazindione **PD**.

Results and Discussion

Synthesis and Self-Assembly of SQ1. The synthetic approach towards squaraine dye **SQ1**, tetralactam macrocycle **MC1** and 1,4-dodecyl-2,5-piperazindione **PD** is shown in Scheme S1 including detailed synthetic procedures and characterization of all new compounds. For the self-assembly studies of **SQ1** by UV/vis spectroscopy, all samples were firstly dissolved in 1,1,2,2-tetrachloroethane (TCE) and then diluted with methylcyclohexane (MCH) in a solvent ratio of MCH:TCE (99:1, v/v). The highly non-polar environment supports the self-assembly by stronger intermolecular interactions.[40] For **SQ1**, at 298 K a transformation (Figure 2b) from a metastable, kinetic aggregate species (**SQ1-Agg1**, λ_{max} = 560 nm) into a thermodynamic aggregate **SQ1-Agg2** was observed (λ_{max} = 661 nm). Further understanding of the self-assembly mechanism and structure of **SQ1-Agg1** were hindered by the instability of said species, since the transformation into **SQ1-Agg2** started without lag time. To shed light on the aggregation behaviour of **SQ1-Agg2**, detailed analysis by temperature- and concentration-dependent UV/vis spectroscopy was performed. The data from several temperature-dependent UV/vis measurements from 293 K to 363 K of **SQ1-Agg2** in MCH:TCE (99:1, v/v) at different total concentrations (c_T) from 7.5×10^{-6} M to 15×10^{-6} M, was fitted with the nucleation-elongation model (Figure S3, for details see SI).[41] The calculated results for the elongation temperature T_E and the enthalpy release ΔH_E upon elongation are summarized in Figure S1c. By van't Hoff analysis (Figure S3d) a standard enthalpy of $\Delta H° = -67.3$ kJ mol^{-1} and a standard entropy of $\Delta S° = -101.6$ J mol^{-1} K^{-1} were estimated. The cooperative self-assembly mechanism of **SQ1-Agg2** was validated by performing concentration-dependent UV/vis measurements in MCH:TCE (99:1, v/v) over a range of $c_T = 2.5 \times 10^{-7}$ M to 8.06×10^{-5} M (Figure S4).

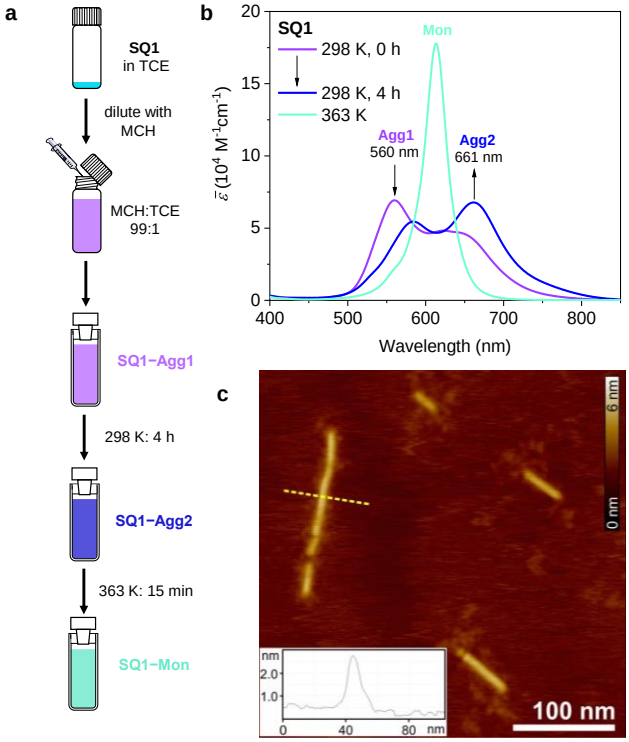

Figure 2. a) Sample preparation procedure towards **SQ1-Agg2**. b) UV/Vis absorption spectra of **SQ1** in MCH:TCE (99:1, v/v, c_T = 20×10^{-6} M) at 298 K directly after sample preparation (**Agg1**), after 4 h at 298 K (**Agg2**) and after heating to 363 K (**Mon**). c) AFM height image of a sample of **SQ1-Agg2** ($c_T = 20 \times 10^{-6}$ M, MCH:TCE, 99:1, v/v) on HOPG.

To gain deeper insights into the packing structure of **SQ1-Agg2**, atomic force microscopy (AFM) measurements were carried out. AFM height images of a sample of **SQ1-Agg2** on Highly Ordered Pyrolytic Graphite (HOPG) show the formation of rigid fiber-like aggregates with the diameter of 2.0±0.3 nm (Figure 2c), the length of the aggregates varies between 18−180 nm. In combination with UV/vis and FT-IR spectroscopy (Figure S7), some conclusions about the packing

arrangement can be drawn. The spectral "double hump" shape of **SQ1-Agg2** (and also **SQ1-Agg1**) with both a hypso- and a bathochromically shifted absorption band with respect to the monomer absorption band is commonly found for thin films of similar aniline-substituted squaraine dyes.[42] It is explained by the presence of both Coulomb and charge transfer couplings in a slip-stacked arrangements of the squaraine chromophores where the donor and acceptor units are positioned on top of each other (for details, see Figure S8).[43,44]

Binding Studies with MC1. The formation of 1:1 complexes between **MC1** and **SQ1** was studied by ^{1}H-NMR and UV/vis titration experiments.[45] For **MC1** and **SQ1**, our studies yielded a binding constant of K = 1.1 × 10^3 M^{-1} in $CDCl_3$ at 295 K (Figure S9), whilst UV/Vis titrations of **MC1** and **SQ1** in toluene led to an increased binding constant of K = 7.4 × 10^3 M^{-1} at 298 K in (Figure S10, ^{1}H-NMR studies in toluene-d_8 were not possible due to the aggregation of **SQ1** at higher concentrations). The observed shifts in the ^{1}H-NMR and UV/vis studies of **SQ1** and **MC1** show similar trends to reported squaraine-tetralactam macrocycle-rotaxane complexes (Figure S14 and S15a).[38,46] Single crystal X-ray diffraction of a co-crystal of bis(*N*,*N*-diethylaniline)squaraine (**SQ3**) and tetralactam-macrocycle **MC2** (similar macrocycle scaffold compared to **MC1**, but without long alkyl chains) showed that the squaraine chromophore fits well into the cavity of the macrocycle (Figure 3, Figure S16 and Table S1). Four hydrogen bonds are formed from the amide protons of **MC2** to the oxygen atoms at the squarylium core of **SQ3** (red dashed lines). The distances d(N···O) range from 2.97 to 3.18 Å indicating that moderate to strong hydrogen bonding takes place.[47]

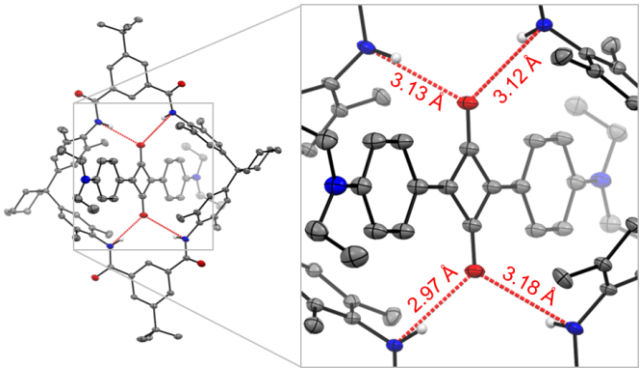

Figure 3. Molecular structure of **SQ3⊂MC2** according to single-crystal X-ray analysis. Between the oxygen atoms at the squarylium core of **SQ3** and the amide protons of the macrocycle **MC2** four hydrogen bonds are formed (red dashed lines). The ellipsoids are set to 50 % probability (C: gray, O: red, N: blue, H: white). Solvent molecules and hydrogen atoms (except for N*H*$_{amide}$ of **MC2**) are omitted for clarity).

For the binding of **PD** by **MC1**, isothermal titration calorimetry (ITC) titration experiments gave about one order of magnitude higher binding constants of K = 3.1 × 10^4 M^{-1} in $CHCl_3$ at 298 K and K = 7.1 × 10^4 M^{-1} in toluene at 298 K (Figure S11, ^{1}H-NMR titration experiments were not possible due to signal broadening in the slow exchange regime at 298 K). Whilst for both complexes the increase of the constant is modest upon changing the solvent from chloroform to toluene, a significantly increased binding strength can be expected in very non-polar solvent mixtures like MCH:TCE (99:1, v/v) as used in the following UV/vis studies.[40] Binding experiments in such non-polar solvents proved to be impossible due to the aggregation of **SQ1** as well as a limited solubility of **MC1** and **PD**. Importantly, the binding studies show that the interaction between **MC1** and **PD** is significantly stronger compared to the binding affinity of **MC1** and **SQ1**. This is a crucial requirement since an initiation of supramolecular polymerization after the kinetic trapping of **SQ1** requires a dethreading of **MC1** from **SQ1**.

Sequestration of SQ1 and Controlled Release. For the kinetic trapping experiments, samples were prepared by dissolving **SQ1** and **MC1** (1:3) in TCE and subsequent dilution with MCH to give a solvent ratio of MCH:TCE (99:1, v/v, c_T(**SQ1**)= 10 × 10^{-6} M, Figure 4a). Time-dependent UV/Vis absorption measurements of this sample, hereafter denoted as **SQ1⊂MC1**, at 293 K show a sharp absorption band at λ_{max} = 635 nm (Figure 4b). The addition of three equivalents of **MC1** successfully trapped **SQ1** in its monomeric form over an extended time period and effectively suppressed spontaneous self-assembly (Figure S15b). Height AFM images on Highly Ordered Pyrolytic Graphite (HOPG) showed the formation of spherical nanoparticles with a diameter of 1.1 ± 0.1 nm (Figure 4d) and a co-agglomeration tendency, but no fibrous aggregates could be observed. In comparison, a sample with only **SQ1** leads to the immediate initiation of self-assembly into aggregate fibers upon dilution with MCH, as discussed before (Figure 2).

In order to initiate the supramolecular polymerization of **SQ1**, a highly concentrated solution of 50 eq. **PD** in MCH:TCE (99:1, v/v) was added to **SQ1⊂MC1**. Immediately afterwards, a time-dependent UV/vis measurement was started and significant spectral changes were instantly observable (Figure 4e): the absorption band of the trapped **SQ1** monomers at λ_{max} = 635 nm diminished drastically and a new hypsochromically shifted band around 560 nm rose (belonging to **SQ1-Agg1**). Over time, the characteristic band shape of **SQ1-Agg2** evolved and full aggregation could be reached (inset, Figure 4e). AFM measurements on HOPG showed the formation of fiber-like aggregates with a diameter of 2.0 ± 0.3 nm (Figure 4g), as expected for **SQ1-Agg2**.

Living Supramolecular Polymerization of SQ1. To investigate the living supramolecular polymerization (LSP) characteristics of the present system, multi-cycle seeding experiments were performed according to the experimental protocol shown in Figure 5a (see also SI). Beforehand, a sample of **SQ1⊂MC1** was prepared in MCH:TCE (99:1, v/v). To this solution, 50 eq. of **PD** were added in order to initiate the supramolecular polymerization into aggregate **SQ1-Agg2**. After equilibration, the **SQ1-Agg2** sample was sonicated for 15 min at 293 K to generate small aggregate fragments, hereafter denoted as **SQ1-Agg2$_{Seed}$**. Then, the solutions with 2 eq. of **SQ1-Agg2$_{Seed}$** (still containing **PD** as initiator) and 1 eq. of **SQ1⊂MC1** (1:3) were mixed and the supramolecular polymerization started immediately (cycle 1). After the first cycle, 1 eq. of the supramolecular polymer solution was removed to keep the sample volume constant. The remaining sample (2 eq.) now acted as seed for cycle 2 and 1 eq. of **SQ1⊂MC1** (1:3) was added. This procedure was repeated for another 2 cycles.

The UV/vis absorption spectra showed that after each addition of trapped monomers the supramolecular polymerization into **SQ1-Agg2** started (Figure 5b). Taking a

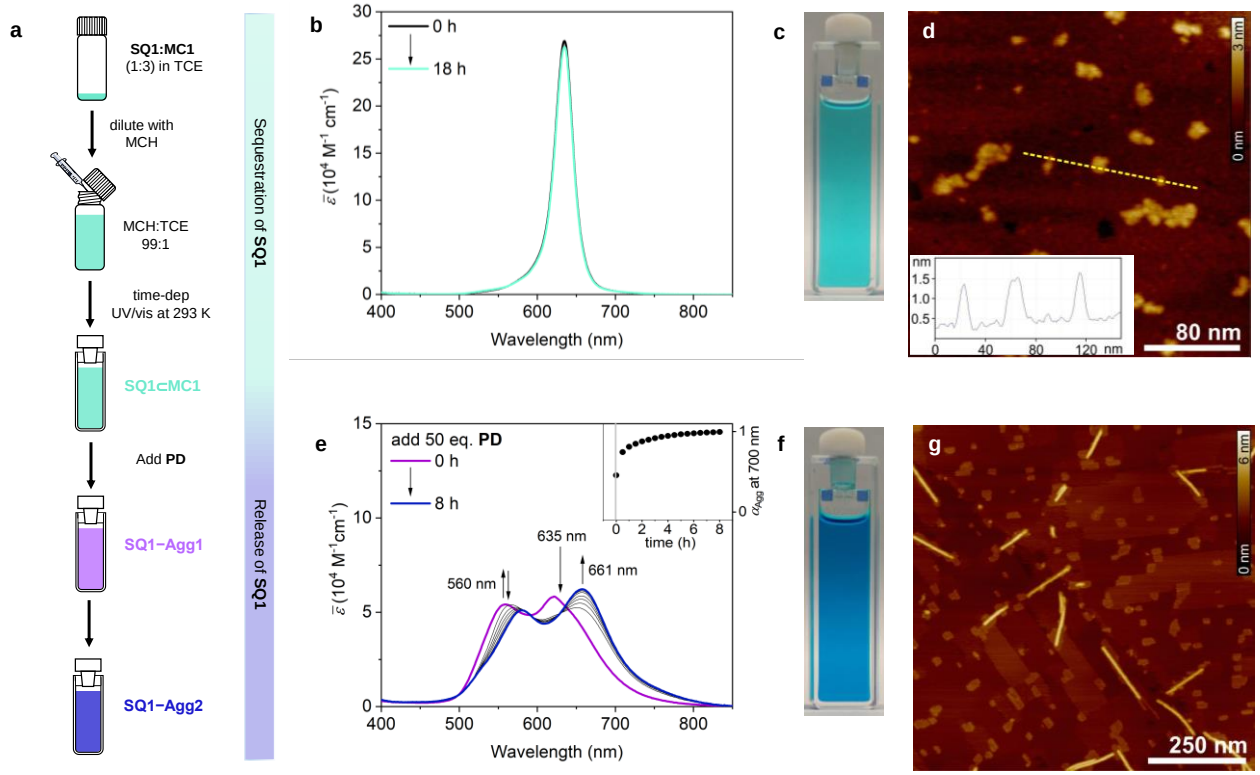

Figure 4. a) Sample preparation procedure for kinetic trapping and controlled release experiments. b) Time-dependent UV/Vis absorption spectra of **SQ1⊂MC1** (1:3, c_T(**SQ1**)= 10 × 10^{-6} M) in MCH:TCE (99:1, v/v) at 293 K and picture of the cuvette (c) after 18 h. d) Height AFM images of the spin-coated sample from (b) on HOPG. Z scale is 3 nm. Inset: cross-section analysis from the dashed line in image (d). e) Time-dependent UV/Vis absorption spectra of **SQ1⊂MC1** (1:3, c_T(**SQ1**)= 10 × 10^{-6} M) in MCH:TCE (99:1, v/v) at 293 K after addition of 50 eq. **PD** (grey spectra: every 60 min) and picture (f) of the cuvette after 8 h. Inset: Plot of the degree of aggregation α_{Agg} at 700 nm against time. The grey line marks the time frame of the addition of 50 eq. of **PD**. g) Height AFM images of the sample from (e) spin-coated on HOPG. Z scale is 6 nm. The island-like structures in the AFM images can be attributed to excess **MC1** and **PD** molecules.

closer look at the time-dependent UV/vis spectra of cycle 1 (Figure 5c), isosbestic points are observable at 587 and 651 nm and no formation of **SQ1-Agg1** was detected. This indicates that only two species are involved in the process and the monomers directly assembled into **SQ1-Agg2** under the control of **MC1** molecular chaperone. Thus, the already present **SQ1-Agg2** aggregates acted as seeds for the polymerization of trapped **SQ1** upon addition of **PD**.

The rate of the polymerization into **SQ1-Agg2** became slower with each cycle because the number of "active termini" of the seed was reduced by one-third with each cycle. This behaviour can be confirmed by plotting the initial slopes[48] (Figure S17b) against the cycle number n and fitted with the exponential equation y = 0.00582 min^{-1} × $(2/3)^{n-1}$, showing the decrease of the initial slope by one-third with each cycle (Figure S17c). Simultaneously, the fiber length should increase with each cycle. AFM height images of spin-coated samples were taken after each cycle, and the fiber length was analysed and visualized in histograms, showing a successive fiber growth (Figure 5d-g, Figure S17a). Starting from a length distribution of **SQ1-Agg2**$_{Seed}$ from 12 to 250 nm, a prolongation of the fibers to 22 to 308 nm (cycle 1) and 28 to 380 nm (cycle 2) was found. After the third cycle, even longer fibers up to a length of 36 to 499 nm could be observed. Additionally, the dispersity of the supramolecular polymers seems to decrease upon iterative addition of the seeds, which further indicates the livelyness of the supramolecular polymerization.

Supramolecular Block Copolymers. As a next step, the controlled formation of supramolecular block copolymers (BCP) was elucidated. For this purpose squaraine dye **SQ2** with an extended linker was synthesized, characterized and investigated concerning it's self-assembly behaviour and binding strength towards **MC1** (Figures S5, S6, S12, S13 and S18). UV/vis spectroscopy studies revealed that the aggregate species **SQ2-Agg2** exhibited a more bathochromically shifted absorption band at λ_{max} = 723 nm (Figure 6c, red dashed line) which suggests an aggregate structure with less CT but more J-type Coulomb coupling as schematically illustrated in Figure S8 (for further information see SI).[44] AFM height images on HOPG show for **SQ2-Agg2** the formation of fiber-like aggregates with a larger diameter of 4.0 ± 0.3 nm (Figure S5) compared to **SQ1-Agg2**.

BCP samples composed of **SQ1** and **SQ2** were prepared according the experimental procedure in Figure 6d. A trapped sample of **SQ2⊂MC1** (1:3) was prepared and aggregation was initiated by addition of **PD** (Figure 6a). Next the equilibrated **SQ2-Agg2** sample was sonicated for 15 min to generate **SQ2-Agg2**$_{Seed}$ (Figure 6e) and then mixed with **SQ1⊂MC1** in a 1 to 1 ratio and monitored by time-dependent UV/vis spectroscopy (Figure 6b). In Figure 6c the resulting experimental spectrum of the BCP (solid orange line), the spectra of the homopolymers **SQ1-Agg2** (dashed blue line) and **SQ2-Agg2** (dashed red line) and a calculated superposition of a 1:1 mixture of both

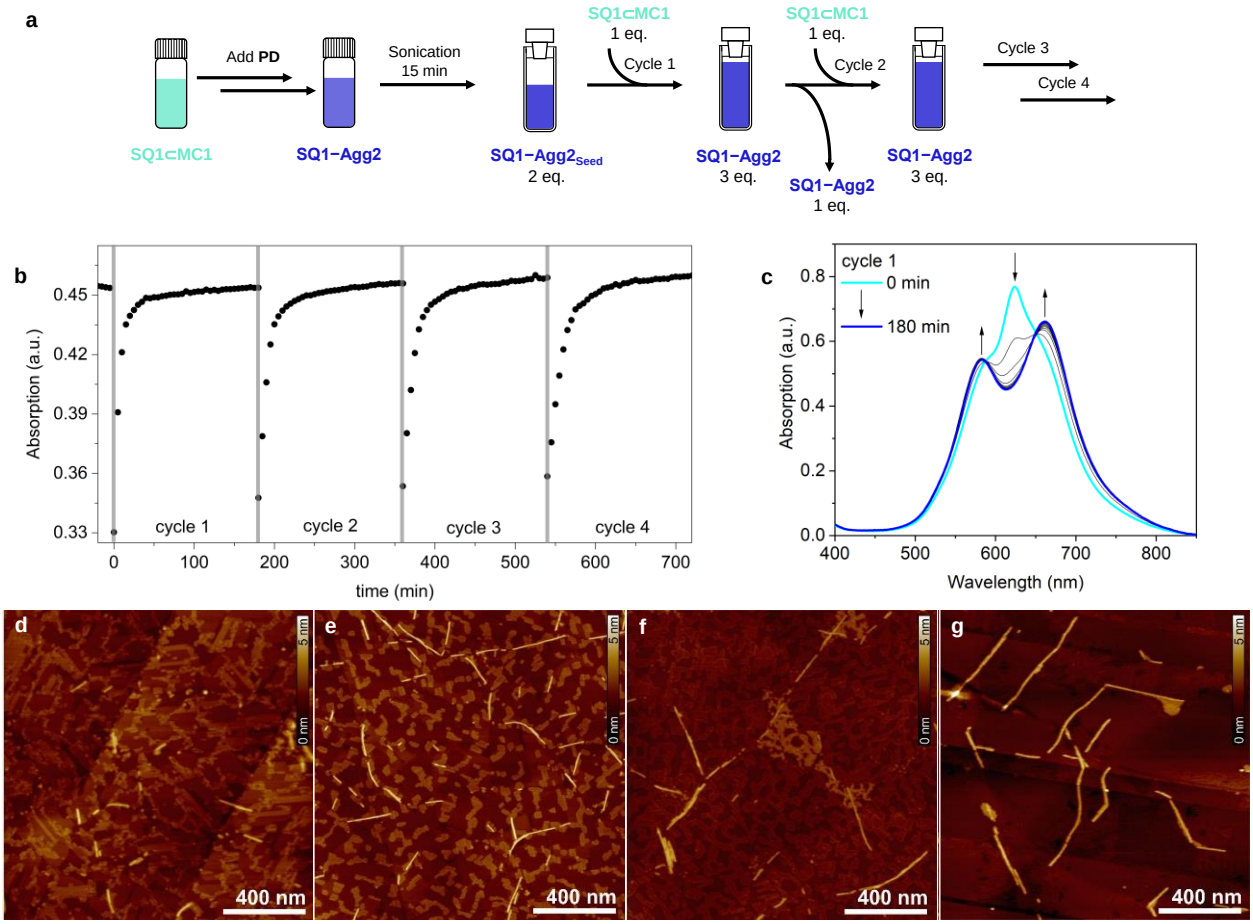

Figure 5. a) Sample preparation procedure for LSP experiments. b) Time-dependent plot of the absorption at λ = 690 nm at 293 K in MCH/TCE (99:1, v/v) during the LSP experiment of **SQ1**. c) Time-dependent UV/vis absorption spectra of "cycle 1" at 293 K in MCH/TCE (99:1, v/v) (grey spectra: every 20 min). d–g) AFM height images of the **SQ1–Agg2$_{Seeds}$** (d) and the supramolecular polymers obtained after the first (e), second (f), third cycle (g) on HOPG. The island-like structures can be attributed to excess **MC1** and **PD** molecules. The Z scale is 5 nm.

homopolymers (dashed orange line) is compared. For a supramolecular block copolymer structure, the extended π-stacks between the individual components should dominate the UV/vis absorption spectrum compared to the absorption from interface areas and indeed the experimental spectrum of the BCP **SQ1**:**SQ2** (1:1, seed: **SQ2**) matched the calculated superposition of **SQ1**-**Agg2** and **SQ2**-**Agg2** (Figure 6c, dashed orange line) well.

Subsequently, AFM studies were carried out to further substantiate the supramolecular block structure. AFM height images on HOPG (Figure 6f and g, Figure S19c-e) show fiber-like aggregates with different heights along the strand (marked with blue and red arrows in Figure 6g). The alternating diameter along the aggregates varies between 2.0 ± 0.3 nm (blue, Figure 6f inset) and 3.9 ± 0.4 nm (red). Over time, long BCP fibers with alternating blocks are observable (Figure S19e), suggesting that the BCP formation mechanism seems to be not only driven by the seeded growth but over time also by fusion (for further information see SI).

A random copolymerization study with **SQ1** and **SQ2** was carried out as a control experiment. Here a sample containing with **SQ1⊂MC1** and **SQ2⊂MC1** was prepared and supramolecular polymerization was initiated by addition of **PD**. The time-dependent UV/vis measurement showed no BCP formation (grey line in Figure 6c and S20b). AFM studies corroborate these results, with AFM height images of spin-coated samples on HOPG showing the formation of short rod-like aggregates with a diameter of 2.0 ± 0.2 nm that indicate no supramolecular block copolymer formation (Figure S20c).

Comparison with Chaperones in Nature. In nature, molecular chaperones often do not act alone but rather as multicomponent molecular machines with ATP and cofactor regulated binding and release cycles.[29] Each component has a specific role and the versatility of molecular chaperones is very high. We focus in this work on one aspect of chaperones, which is the suppression of premature self-assembly of monomers units.[49,50] In a similar way, a variety of chaperones aids the self-assembly of flagella on the bacterial cell surface, a long tubular filament consisting of ca. 20,000 monomer units. Inside

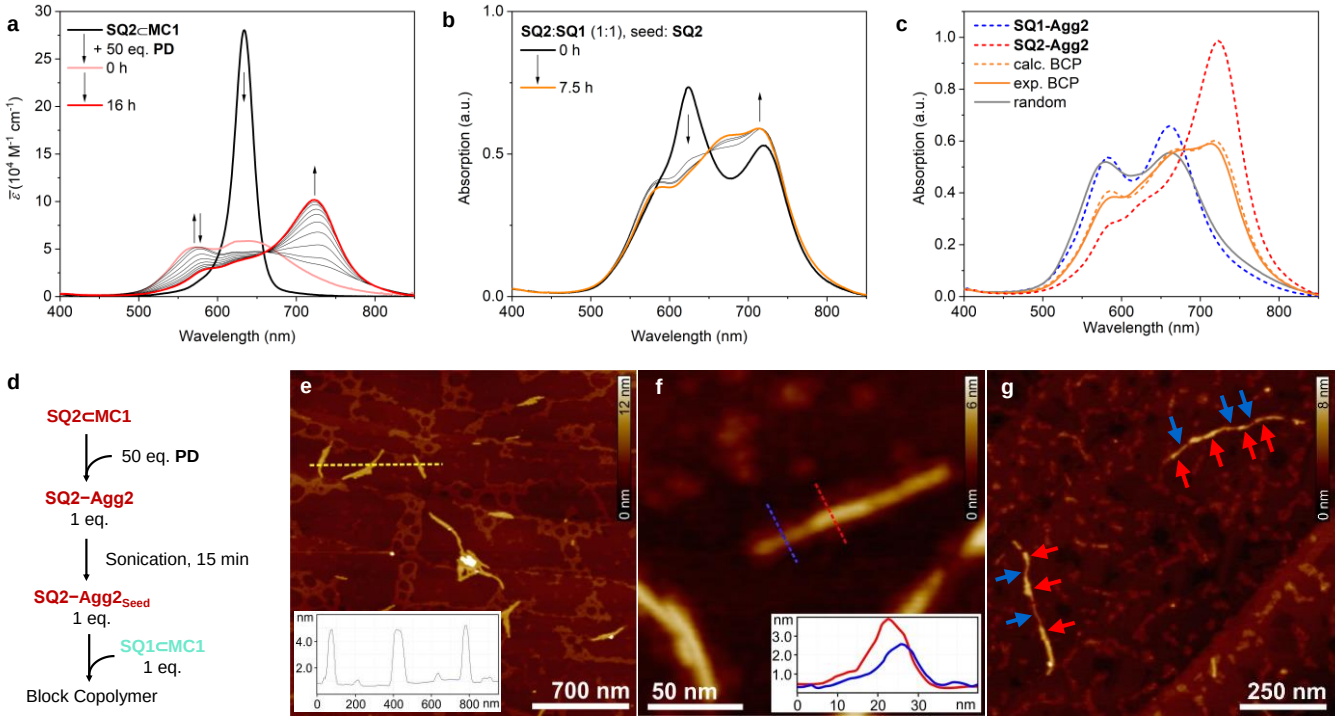

Figure 6. a) Time-dependent UV/vis absorption spectra of the initiation of supramolecular polymerization of **SQ2⊂MC1** (**SQ2**:**MC1**, 1:3, c_T(**SQ2**) = 1× 10^{-5} M) by addition of 50 eq. of **PD** in MCH:TCE (99:1, v/v) at 293 K. b) Time-dependent UV/vis absorption spectra of the block copolymerization experiment with **SQ2** and **SQ1** (1:1, **SQ2** as seed, c_T(**SQ2**)= 5 × 10^{-6} M) in MCH:TCE (99:1, v/v) at 293 K. c) Comparison of UV/vis absorption spectra in MCH:TCE (99:1, v/v, c_T(**SQ**) = 1 × 10^{-5} M) at 293 K of **SQ1-Agg2** (blue dash) and **SQ2-Agg2** (red dash), the calc. superposition of **SQ1-Agg2**:**SQ2-Agg2** (1:1, orange dash), the experimental BCP (**SQ1**:**SQ2**, 1:1, orange) and the random copolymer (**SQ1**:**SQ2** (1:1), grey). d) Sample preparation procedure for BCP experiments. e) Height AFM images of **SQ2-Agg2**$_{\mathbf{Seed}}$ in MCH:TCE (99:1, v/v, c_T(**SQ2**) = 1 × 10^{-5} M) prepared by spin-coating the solution directly after ultrasonication on HOPG. Z scale is 12 nm. The island-like structures could be related to excess **MC1** and **PD**. Inset shows the cross section analyses of the seeds with diameters around 3.9±0.2 nm. f and g) Height AFM images of the BCP with **SQ2** and **SQ1** (1:1, c_T(**SQ**) = 1 × 10^{-5} M) in MCH:TCE (99:1, v/v) prepared by spin-coating the solution on HOPG. Z scale is 6 nm (f) and 8 nm (g). The island-like structures could be related to excess **MC1** and **PD**. Inset shows the cross section analyses at two different positions of the fibre.

the cell, the newly synthesized subunits are captured by substrate specific molecular chaperones to prevent premature self-assembly in the cytoplasm. Only after transport to the export gate in the cell membrane, the monomers travel through the extracellular filament structure and assemble at the nascent end of the flagella.[49] Similarities to our system can be found: Initially **MC1** sequesters **SQ1** and thereby suppressed spontaneous nucleation of monomers into undesired amorphous aggregate species (**SQ1-Agg1**). Instead only through addition of **PD** (acting as binding regulating co-factor), the substrate **SQ1** was released and self-assembly proceeded into desired fiber aggregates (**SQ1-Agg2**) in the presence of seeds. Analogous to molecular chaperones, **MC1** and **PD** are not present in the final structure and don't give information for the correct self-assembly. In general, molecular assembly chaperones in nature often show a selective activity, while folding chaperones usually cover a broad range of substrates with few client-specific chaperones.[29,30] In our system, the structural motif of the central squaric acid unit of the squaraine dye core is essential for strong interaction with the tetralactam macrocycle, leading to a selective interaction through hydrogen-bonding.

Conclusion

In this paper, we demonstrated how an artificial chaperone-like macrocyclic receptor could be used to control the supramolecular polymerization of a squaraine dye. Exploiting a kinetic trapping strategy by complexation and controlled release of a squaraine dye by the macrocycle receptor, the spontaneous supramolecular polymerization of the squaraine dye was regulated and precise control over the timing of the self-assembly process by an initiator molecule could be achieved. Thus, we could show how such molecular chaperone strategy found in nature can be utilized to control living supramolecular polymerizations and supramolecular block copolymer synthesis, demonstrating a new possibility for the precise control of self-assembly processes by means of synthetic molecular chaperone analogues.

ASSOCIATED CONTENT

Supporting Information. The Supporting Information is available on the ACS Publications website at DOI: http://pubs.acs.org.

Experimental methods, synthetic procedures and characterization of new compounds, additional aggregation studies of squaraine dyes by UV/vis spectroscopy, FTIR spectroscopy, determination of binding constants, single crystal X-ray analysis of co-crystal,

seeded supramolecular (co-)polymerization by UV/vis spectroscopy and AFM, NMR spectra for the new compounds.

Accession Code CCDC 2210252 contains the supplementary crystallographic data for this paper. These data can be obtained free of charge via www.ccdc.cam.ac.uk/data_request/cif, or by emailing data_request@ccdc.cam.ac.uk, or by contacting The Cambridge Crystallographic Data Centre, 12 Union Road, Cambridge CB2 1EZ, UK; fax: +44 1223 336033.

Data Availability Statement. Additional spectroscopic data underlying this study are openly available in Zenodo at 10.5281/zenodo.7777196.

AUTHOR INFORMATION

Corresponding Author

* **Frank Würthner** – *Institut für Organische Chemie, Universität Würzburg, Würzburg 97074, Germany; Center for Nanosystems Chemistry (CNC), Universität Würzburg, Würzburg 97074, Germany*; orcid.org/0000-0001-7245-0471;
Email: wuerthner@uni-wuerzburg.de

Authors

† **Lara Kleine-Kleffmann** – *Institut für Organische Chemie, Universität Würzburg, Würzburg 97074, Germany;*

†,‡ **Vladimir Stepanenko** – *Institut für Organische Chemie, Universität Würzburg, Würzburg 97074, Germany; Center for Nanosystems Chemistry (CNC), Universität Würzburg, Würzburg 97074;* orcid.org/0000-0001-7994-823X.

‡ **Kazutaka Shoyama** – *Center for Nanosystems Chemistry (CNC), Universität Würzburg, Würzburg 97074*, orcid.org/0000-0003-0937-4431.

† **Marius Wehner** – *Institut für Organische Chemie, Universität Würzburg, Würzburg 97074, Germany;*

Author Contributions

All authors have given approval to the final version of the manuscript.

Notes

The authors declare no competing financial interest.

ACKNOWLEDGMENT

We thank the Fonds der Chemischen Industrie for a Kekulé fellowship for L.K.-K.. We acknowledge DESY (Hamburg, Germany), a member of the Helmholtz Association HGF, for providing experimental facilities at PETRA III (proposal No STP-20211168). We thank Dr. Eva Crosas for assistance in using P11.

REFERENCES

(1) Amabilino, D. B.; Smith, D. K.; Steed, J. W. Supramolecular materials. *Chem. Soc. Rev.* **2017**, *46*, 2404−2420.
(2) Kassem, S.; van Leeuwen, T.; Lubbe, A. S.; Wilson, M. R.; Feringa, B. L.; Leigh, D. A. Artificial molecular motors. *Chem. Soc. Rev.* **2017**, *46*, 2592−2621.
(3) Yang, L.; Tan, X.; Wang, Z.; Zhang, X. Supramolecular Polymers: Historical Development, Preparation, Characterization, and Functions. *Chem. Rev.* **2015**, *115*, 7196−7239.
(4) Aida, T.; Meijer, E. W.; Stupp, S. I. Functional Supramolecular Polymers. *Science* **2012**, *335*, 813−817.
(5) De Greef, T. F. A.; Smulders, M. M. J.; Wolffs, M.; Schenning, A. P. H. J.; Sijbesma, R. P.; Meijer, E. W. Supramolecular Polymerization. *Chem. Rev.* **2009**, *109*, 5687−5754.
(6) Wojtecki, R. J.; Meador, M. A; Rowan, S. J. Using the dynamic bond to access macroscopically responsive structurally dynamic polymers. *Nat. Mater.* **2011**, *10*, 14−27.
(7) Webber, M. J.; Appel, E. A.; Meijer, E. W.; Langer, R., Supramolecular biomaterials. *Nature Materials* **2016,** *15*, 13−26.
(8) Fouquey, C.; Lehn, J.-M.; Levelut, A.-M. Molecular recognition directed self-assembly of supramolecular liquid crystalline polymers from complementary chiral components. *Adv. Mater.* **1990**, *2*, 254−257.
(9) Matern, J.; Dorca, Y.; Sánchez, L.; Fernández, G., Revising Complex Supramolecular Polymerization under Kinetic and Thermodynamic Control. *Angew. Chem. Int. Ed.* **2019,** *58*, 16730−16740.
(10) Wehner, M.; Würthner, F., Supramolecular polymerization through kinetic pathway control and living chain growth. *Nat. Rev. Chem.* **2020,** *4*, 38−53.
(11) Sorrenti, A.; Leira-Iglesias, J.; Markvoort, A. J.; de Greef, T. F. A.; Hermans, T. M., Non-equilibrium supramolecular polymerization. *Chem. Soc. Rev.* **2017,** *46*, 5476−5490.
(12) Mattia, E.; Otto, S., Supramolecular systems chemistry. *Nat. Nanotechnol.* **2015,** *10*, 111−119.
(13) Korevaar, P. A.; George, S. J.; Markvoort, A. J.; Smulders, M. M. J.; Hilbers, P. A. J.; Schenning, A. P. H. J.; De Greef, T. F. A.; Meijer, E. W. Pathway complexity in supramolecular polymerization. *Nature* **2012**, *481*, 492−496.
(14) Kang, J.; Miyajima, D.; Mori, T.; Inoue, Y.; Itoh, Y.; Aida, T. A rational strategy for the realization of chain-growth supramolecular polymerization. *Science* **2015**, *347*, 646−651.
(15) Ogi, S.; Sugiyasu, K.; Manna, S.; Samitsu, S; Takeuchi, M. Living supramolecular polymerization realized through a biomimetic approach. *Nat. Chem.* **2014**, 6, 188−195.
(16) Ogi, S.; Stepanenko, V.; Sugiyasu, K.; Takeuchi, M.; Würthner, F., Mechanism of Self-Assembly Process and Seeded Supramolecular Polymerization of Perylene Bisimide Organogelator. *J. Am. Chem. Soc.* **2015,** *137*, 3300−3307.
(17) Endo, M.; Fukui, T.; Jung, S. H.; Yagai, S.; Takeuchi, M.; Sugiyasu, K., Photoregulated Living Supramolecular Polymerization Established by Combining Energy Landscapes of Photoisomerization and Nucleation–Elongation Processes. *J. Am. Chem. Soc.* **2016,** *138*, 14347−14353.
(18) Kar, H.; Ghosh, G.; Ghosh, S., Solvent Geometry Regulated Cooperative Supramolecular Polymerization. *Chem. Eur. J.* **2017,** *23*, 10536−10542.
(19) Datta, S.; Kato, Y.; Higashiharaguchi, S.; Aratsu, K.; Isobe, A.; Saito, T.; Prabhu, D. D.; Kitamoto, Y.; Hollamby, M. J.; Smith, A. J.; Dalgliesh, R.; Mahmoudi, N.; Pesce, L.; Perego, C.; Pavan, G. M.; Yagai, S., Self-assembled poly-catenanes from supramolecular toroidal building blocks. *Nature* **2020,** *583*, 400−405.
(20) Ogi, S.; Matsumoto, K.; Yamaguchi, S., Seeded Polymerization through the Interplay of Folding and Aggregation of an Amino-Acid-based Diamide. *Angew. Chem. Int. Ed.* **2018,** *57*, 2339−2343.
(21) Jalani, K.; Das, A. D.; Sasmal, R.; Agasti, S. S.; George, S. J., Transient dormant monomer states for supramolecular polymers with low dispersity. *Nat. Commun.* **2020,** *11*, 3967
(22) Fukui, T.; Kawai, S.; Fujinuma, S.; Matsushita, Y.; Yasuda, T.; Sakurai, T.; Seki, S.; Takeuchi, M.; Sugiyasu, K., Control over differentiation of a metastable supramolecular assembly in one and two dimensions. *Nat. Chem.* **2017,** *9*, 493−499.
(23) Greciano, E. E.; Matarranz, B.; Sánchez, L., Pathway Complexity Versus Hierarchical Self-Assembly in N-Annulated Perylenes:

Structural Effects in Seeded Supramolecular Polymerization. *Angew. Chem. Int. Ed.* **2018,** *57*, 4697−4701.
(24) Sarkar, S.; Sarkar, A.; George, S. J., Stereoselective Seed-Induced Living Supramolecular Polymerization. *Angew. Chem. Int. Ed.* **2020,** *59*, 19841−19845.
(25) Wang, X.; Guerin, G.; Wang, H.; Wang, Y.; Manners, I.; Winnik, M. A., Cylindrical Block Copolymer Micelles and Co-Micelles of Controlled Length and Architecture. *Science* **2007,** *317*, 644−647.
(26) Zhang, W.; Jin, W.; Fukushima, T.; Saeki, A.; Seki, S.; Aida, T., Supramolecular Linear Heterojunction Composed of Graphite-Like Semiconducting Nanotubular Segments. *Science* **2011,** *334*, 340−343.
(27) Wagner, W.; Wehner, M.; Stepanenko, V.; Würthner, F., Supramolecular Block Copolymers by Seeded Living Polymerization of Perylene Bisimides. *J. Am. Chem. Soc.* **2019,** *141*, 12044−12054.
(28) Sarkar, A.; Sasmal, R.; Das, A.; Venugopal, A.; Agasti, S. S.; George, S. J., Tricomponent Supramolecular Multiblock Copolymers with Tunable Composition via Sequential Seeded Growth. *Angew. Chem. Int. Ed.* **2021,** *60*, 18209−18216.
(29) Hartl, F. U.; Bracher, A.; Hayer-Hartl, M., Molecular chaperones in protein folding and proteostasis. *Nature* **2011,** *475*, 324−332.
(30) Ellis, R. J., Assembly chaperones: a perspective. *Philos. Trans. R. Soc. B: Biol. Sci.* **2013,** *368*, 20110398.
(31) Nishimura, T.; Akiyoshi, K., Artificial Molecular Chaperone Systems for Proteins, Nucleic Acids, and Synthetic Molecules. *Bioconj. Chem.* **2020,** *31*, 1259−1267.
(32) Tran, M. L.; Génisson, Y.; Ballereau, S.; Dehoux, C., Second-Generation Pharmacological Chaperones: Beyond Inhibitors. *Molecules* **2020,** *25*, 3145.
(33) Cortez, L.; Sim, V., The therapeutic potential of chemical chaperones in protein folding diseases. *Prion* **2014**, *8*, 197−202.
(34) Chi, X.; Xu, D.; Yan, X.; Chen, J.; Zhang, M.; Hu, B.; Yu, Y.; Huang, F., A water-soluble, shape-persistent, mouldable supramolecular polymer with redox-responsiveness in the presence of a molecular chaperone. *Polym. Chem.* **2013,** *4*, 2767−2772.
(35) Paraschiv, V.; Crego-Calama, M.; Ishi-i, T.; Padberg, C. J.; Timmerman, P.; Reinhoudt, D. N., Molecular "Chaperones" Guide the Spontaneous Formation of a 15-Component Hydrogen-Bonded Assembly. *J. Am. Chem. Soc.* **2002**, *124*, 7638−7639.
(36) Peters, G. M.; Skala, L. P.; Davis, J. T., A Molecular Chaperone for G4-Quartet Hydrogels. *J. Am. Chem. Soc.* **2016,** *138*, 134−139.
(37) Wang, Y.; Sun, Y.; Shi, P.; Sartin, M. M.; Lin, X.; Zhang, P.; Fang, H.; Peng, P.; Tian, Z.; Cao, X., Chaperone-like chiral cages for catalyzing enantio-selective supramolecular polymerization. *Chem. Sci.* **2019,** *10*, 8076−8082.
(38) Dempsey, J. M.; Zhang, Q.-W.; Oliver, A. G.; Smith, B. D., New tetralactam hosts for squaraine dyes. *Org. Biomol. Chem.* **2018,** *16*, 8976−8983.
(39) Dzyuba, E. V.; Kaufmann, L.; Löw, N. L.; Meyer, A. K.; Winkler, H. D. F.; Rissanen, K.; Schalley, C. A., CH···O Hydrogen Bonds in "Clicked" Diketopiperazine-Based Amide Rotaxanes. *Org. Lett.* **2011**, *13*, 18, 4838–4841 .
(40) Würthner, F., Solvent Effects in Supramolecular Chemistry: Linear Free Energy Relationships for Common Intermolecular Interactions. *J. Org. Chem.* **2022,** *87*, 1602−1615.
(41) Jonkheim, P; van der Schoot, P.; Schenning, A. P. H. J.; Meijer, E. W., Probing the Solvent-Assisted Nucleation Pathway in Chemical Self-Assembly. *Science* **2006**, 313, 5783, 80−83.
(42) Zheng, C.; Jalan, I.; Cost, P.; Oliver, K.; Gupta, A.; Misture, S.; Cody, J. A.; Collison, C. J., Impact of Alkyl Chain Length on Small Molecule Crystallization and Nanomorphology in Squaraine-Based Solution Processed Solar Cells. *J. Phys. Chem. C* **2017,** *121*, 7750−7760.
(43) Hestand, N. J.; Zheng, C.; Penmetcha, A. R.; Cona, B.; Cody, J. A.; Spano, F. C.; Collison, C. J., Confirmation of the Origins of Panchromatic Spectra in Squaraine Thin Films Targeted for Organic Photovoltaic Devices. *J. Phys. Chem. C* **2015,** *119*, 18964−18974.
(44) Shen, C.-A.; Bialas, D.; Hecht, M.; Stepanenko, V.; Sugiyasu, K.; Würthner, F., Polymorphism in Squaraine Dye Aggregates by Self-Assembly Pathway Differentiation: Panchromatic Tubular Dye Nanorods versus J-Aggregate Nanosheets. *Angew. Chem. Int. Ed.* **2021,** *60*, 11949−11958.
(45) Thordarson, P., Determining association constants from titration experiments in supramolecular chemistry. *Chem. Soc. Rev.* **2011**, 40, 1305−1323
(46) Gassensmith, J. J.; Barr, L.; Baumes, J. M.; Paek, A.; Nguyen, A.; Smith, B. D., Synthesis and Photophysical Investigation of Squaraine Rotaxanes by "Clicked Capping". *Org. Lett.* **2008,** *10*, 3343−3346.
(47) MacLeod, J. M.; Rosei, F., 3.02 - Directed Assembly of Nanostructures. In *Comprehensive Nanoscience and Technology*, Andrews, D. L.; Scholes, G. D.; Wiederrecht, G. P., Eds.; Academic Press: Amsterdam, **2011**; pp 13−68.
(48) Wagner, W.; Wehner, M.; Stepanenko, V.; Ogi, S.; Würthner, F., Living Supramolecular Polymerization of a Perylene Bisimide Dye into Fluorescent J-Aggregates, *Angew. Chem. Int. Ed.* **2017**, 56, 16008−16012.
(49) Bange, G.; Kümmerer, N.; Engel, C.; Bozkurt, G.; Wild, K.; Sinning, I., FlhA provides the adaptor for coordinated delivery of late flagella building blocks to the type III secretion system. *Proc. Natl. Acad. Sci.* **2010,** *107*, 11295−11300.
(50) Soto, G. E.; Dodson, K. W.; Ogg, D.; Liu, C.; Heuser, J.; Knight, S.; Kihlberg, J.; Jones, C. H.; Hultgren, S. J., Periplasmic chaperone recognition motif of subunits mediates quaternary interactions in the pilus. *EMBO J.* **1998**, 17, 6155−6167.